water

MDPI

Article

Delineation of a Quaternary Aquifer Using Integrated Hydrogeological and Geophysical Estimation of Hydraulic Conductivity on the Tibetan Plateau, China

Tuong Vi Tran [1,*], Johannes Buckel [2], Philipp Maurischat [3], Handuo Tang [4], Zhengliang Yu [4], Andreas Hördt [2], Georg Guggenberger [3], Fan Zhang [4], Antje Schwalb [5] and Thomas Graf [1]

1 Institute of Fluid Mechanics and Environmental Physics in Civil Engineering, Leibniz Universität Hannover, Appelstr. 9A, 30167 Hannover, Germany; graf@hydromech.uni-hannover.de
2 Institute for Geophysics and Extraterrestrial Physics, Technische Universität Braunschweig, Mendelssohnstr. 3, 38106 Braunschweig, Germany; j.buckel@tu-braunschweig.de (J.B.); a.hoerdt@tu-braunschweig.de (A.H.)
3 Institute of Soil Science, Leibniz Universität Hannover, Herrenhäuser Str. 2, 30419 Hannover, Germany; maurischat@ifbk.uni-hannover.de (P.M.); guggenberger@ifbk.uni-hannover.de (G.G.)
4 Key Laboratory of Tibetan Environment Changes and Land Surface Processes, Institute of Tibetan Plateau Research, Chinese Academy of Sciences, Beijing 100049, China; tanghanduo@itpcas.ac.cn (H.T.); yuzhengliang@itpcas.ac.cn (Z.Y.); zhangfan@itpcas.ac.cn (F.Z.)
5 Institute of Geosystems and Bioindication, Technische Universität Braunschweig, Langer Kamp 19C, 38106 Braunschweig, Germany; antje.schwalb@tu-bs.de
* Correspondence: tran@hydromech.uni-hannover.de; Tel.: +49-511-762-3568

Citation: Tran, T.V.; Buckel, J.; Maurischat, P.; Tang, H.; Yu, Z.; Hördt, A.; Guggenberger, G.; Zhang, F.; Schwalb, A.; Graf, T. Delineation of a Quaternary Aquifer Using Integrated Hydrogeological and Geophysical Estimation of Hydraulic Conductivity on the Tibetan Plateau, China. *Water* **2021**, *13*, 1412. https://doi.org/10.3390/w13101412

Academic Editor: Francesco Fiorillo

Received: 30 March 2021
Accepted: 13 May 2021
Published: 18 May 2021

Abstract: Groundwater is the most unexplored element of the hydrologic cycle on the Tibetan Plateau (TP) due to harsh climate conditions. This study aims at delineating and characterizing the unexplored Zhanongtang–Ganmanong aquifer, situated in the Zhagu subcatchment of the Nam Co catchment, south-central TP. Multiple hydrogeophysical and lithological in situ field and laboratory methods are applied: depth-to-water-table measurements, grain size analysis, hydraulic empirical and field methods to estimate hydraulic conductivity (K), and analysis of electrical resistivity tomography profiles. Integration of these methods revealed the existence of a Quaternary hydrostratigraphic unit that was found to be unconsolidated, laterally heterogeneous and homogeneous over depth. The results revealed consistent K ranges of three K zones, which is in accordance with local lithology. The K ranges are applicable to other locations within the Nam Co catchment with similar lithology as in the study area without further field experiments. Permafrost was found to be absent in the study area ranging from 4730 m a.s.l. to 5200 m a.s.l. altitude. These results provide insight into the hydrogeological conditions of the TP and are useful for conceptual and numerical groundwater flow modeling to predict future changes of water fluxes and water budgets caused by climatic change, especially in remote areas.

Keywords: Tibetan Plateau; hydrostratigraphy; geophysical methods; hydraulic conductivity; groundwater exploration; aquifer; grain size analysis

1. Introduction

The Tibetan Plateau (TP), also called the Asian Water Tower [1] provides water for billions of people supraregionally in India, Bangladesh, China and Southeast Asia, representing over 20% of the global population [2,3]. Ref. [4] postulated that rivers originating from the central TP are influenced by discharging melt- and groundwater, contributing to significant and variable amounts of water towards streams. This underpins the importance of groundwater from the TP as a globally important fresh water resource. Assessment of regional subsurface structures and the hydrogeologic environment is crucial to understand the hydrologic cycle of the TP, which sustains the water supply to the Asian Water Tower.

To investigate regional groundwater flow systems and runoff characteristics, aquifers and confining beds need to be defined [5]. However, knowledge about hydrostratigraphic units and hydrogeologic properties of many parts of the TP remain unclear due to its remoteness and harsh environment. The present study is therefore motivated by the need to increase knowledge of hydrostratigraphic units and their hydrogeologic characteristics of a remote and ungauged area on the TP. In this article, we demonstrate how these characteristics can be assessed by integrated hydrogeological and geophysical field methods, by laboratory analyses and by empirical mathematical relationships.

For the hydrostratigraphic and hydrogeologic investigations, the Nam Co Lake catchment provides an ideal natural laboratory due to its endorheic character [6]. The Nam Co Lake is the second largest lake on the TP [7]. For this reason, the Institute of Tibetan Plateau and the Chinese Academy of Sciences (ITP-CAS) established the Nam Co Monitoring and Research station for Multisphere Interactions (NAMORS) in June 2005, in order to study geology, hydrology, chemistry, biology, meteorology and ecology on the TP [6,8]. Current hydrological studies have addressed surface water fluxes, e.g., changes in lake levels, runoff and water storage related to climate change [9,10]. Only a few studies have addressed groundwater by focusing on lake water–groundwater flux interactions [11,12] or neglected those exchanges by stating that Nam Co is a closed basin [8].

The impact of climatic change on water fluxes on the TP has been examined over the last several decades. Long-term meteorological records (1961–2015) show increasing air temperature with a rate of 0.04 °C per year from 1961–2015 [13]. This influences the hydrological cycle in multiple ways [13,14]. Ref. [15] analyzed two time periods and observed that the rise of air temperature actually increased from 0.06 °C per year (1991–2000) to 0.13 °C per year (2001–2010). This increase in temperature led to an accelerated glacier shrinkage and permafrost degradation with higher runoff [9,16–20]. Consequently, the lake water level of the Nam Co Lake as well as almost all lakes on the TP has risen. This has been confirmed by remote sensing and GIS data, field surveys and lake balance simulations [21,22]. Lake level changes are also attributed to changing precipitation [14,23–25] and changing lake evaporation [26]. Ref. [9] investigated the relationship between Nam Co Lake level changes and changes in evaporation, precipitation and glacial melt during 2002–2009. They found that the lake level increased by 0.33 m per year between 2003 and 2009, mainly due to increased precipitation (51%) and glacier meltwater (21%).

Various studies have assessed the impact of climate change on the hydrologic cycle by applying hydrological modeling techniques, such as snow runoff melt models, rainfall runoff models, climate data-driven models, degree day models, energy models or SWAT (Soil and Water Assessment Tool) models [16,19,24]. A common method is the calculation of water balances [7,11,14,18,21,25,27–29]. Ref. [18] used remote sensing and GIS techniques to perform a quantitative analysis of the Nam Co Lake surface area and volume variations from 1971 to 2004. The analysis is based on a black box model including an uncertainty term for undefined physical processes such as groundwater flow, melting of frozen soil water and water infiltration. They found that the lake surface area expanded by 5% from 1971 to 2004. [27] used the water balance method and the same uncertainty assumption as [18] and highlighted that the seepage rate out of Nam Co Lake has decreased since 2000. Ref. [11] used the water balance method for the Nam Co Lake to study hydrological processes responding to climate change. However, due to the complete absence of groundwater flux data, groundwater was neglected in the analysis. Nevertheless, a large water imbalance was observed indicating loss of lake water by seepage, corresponding to 5–8 mm per day out of the lake. Ref. [14] used a dynamic monthly water balance model to simulate Nam Co Lake levels from 1980–2010. The hydrogeological connection was represented by a linear relationship between groundwater outflow and water level. It was found that lake level rose from 1980–2010 by 5.93 m. Ref. [13] applied a lumped watershed model to analyze the Nam Co Lake water budget during 1961–2015 and showed that 20% of groundwater seepage contributed to the water loss in the Nam Co Lake. These studies suggest that interactions between lake water and groundwater exist, while the nature of that interaction

remains unclear due to deficient knowledge of hydrostratigraphic units and hydrogeologic characteristics of groundwater systems on the TP.

Attempts to investigate groundwater flow on the TP have been made by [20,30]. Ref. [20] sampled groundwater and conducted isotope analyses. It was indicated that there may be subsurficial pathways across underground fractures and fracture networks between the TP and the Alxa Plateau (Inner Mongolia, China; approximately 1650 km away). Ref. [2] concluded that the large groundwater reservoirs of the TP may be connected to groundwater systems in other regions. These connected groundwater systems are therefore highly dependent on the hydrostratigraphy of the TP. However, to the best of our knowledge, studies of hydrostratigraphic units on the TP have not yet been carried out.

Geophysical methods are widely used to delineate hydrostratigraphic structures [31–34]. Ref. [35] used electrical resistivity tomography (ERT) to delineate water-bearing zones. Ref. [32] used ERT combined with hydrogeological data, here slug and pumping tests, to delineate stratigraphic heterogeneity in a river loop, located close to Tübingen, Germany. In that case, ERT profiles revealed a layered stratigraphic model with a sandy gravel aquifer. Slug tests and pumping tests suggest hydraulic conductivity ranges between 10^{-4} m s^{-1}–10^{-3} m s^{-1} (slug test) and 10^{-2} m s^{-1} (pumping test). These studies showed that ERT profiles in combination with hydrogeological methods are useful to delineate and characterize hydrostratigraphic units. As an endorheic system, the Nam Co catchment is predestined for initial hydrostratigraphic surveys on the TP.

Knowledge of the subsurface sediment structures around the Nam Co Lake is a prerequisite to understand and classify hydrostratigraphic units. First, studies of sediments at Nam Co were carried out by [36], who examined two sediment profiles (2 m and 1.40 m thickness) from the Nam Co terrace. This terrace geomorphologically divides the Nam Co catchment between a lower area close to the lake shore and higher valleys further away from the lake.

Recent studies in the Nam Co Lake catchment mostly focused on lake water–groundwater interactions [11,13]. These studies suggest that the Nam Co Lake groundwater system at the TP may be connected to other remote plateaus by deep groundwater pathways. However, specific knowledge of the hydrostratigraphic units in the Nam Co Lake catchment remains unclear.

The primary goal I of this study is to characterize the regional hydrostratigraphic unit by delineating an aquifer. First, we delineate the Zhanongtang–Ganmanong aquifer using integrated hydrogeological, lithological, geophysical methods and existent geological maps. The second goal II is to assess the hydraulic conductivity distribution in a subcatchment of the TP. The findings will make an important contribution to understanding the hydrogeological subsurface conditions at the Nam Co. Additionally, these findings outline how these combined methods can be applied to other remote areas. To the best of our knowledge, this is the first study that hydrogeologically characterizes a subcatchment of Nam Co on the TP using integrated hydrogeophysical field, laboratory and mathematical methods.

2. Materials and Methods

2.1. Study Area

The study area is located on the Tibetan Plateau (Figure 1a), where the Nam Co Lake (lake center at 30°340′ N, 90°30′ E, [37]) is the second largest lake (Figure 1b). The selected study area is the Zhagu subcatchment (Figure 1c), inside the eastern Nam Co catchment area.

According to the Chinese Meteorological Administration, the Nam Co catchment features a semi-arid subarctic climate [38]. The Nam Co catchment is located in a monsoon transition zone characterized by heavy seasonality. During the summer monsoon months (June–September) the climate is controlled by the Indian Ocean Summer Monsoon distinguished by warm and wet air, while the Westerlies dominate during non-monsoon months (October–May) with cold and dry air [6,39].

The mean annual precipitation is ~415 mm at meteorological station NAMORS. The majority of precipitation occurs as rainfall during summer with ~332 mm (80%), whereas precipitation occurs as snowfall in winter with ~83 mm (20%) [6]. Due to the extreme climate, the area is covered by sparse vegetation and episodically filled streams. Alpine pastures, consisting mainly of the sedge species, *Kobresia pygmaea*, with a strong degree of degradation and alpine steppe are found in the entire study area [8,40,41].

The Nam Co catchment is of tectonic origin, and it includes the Yarlung Zangbo and Bangong-Nujiang suture zones. Both are parts of the Lhasa terrain and rose in late Jurassic to early Cretaceous [42]. The Bangong-Nujiang suture zone is spread over the Cretaceous-Tertiary Gangdese plutonic belt and overlain by volcanic rocks of similar age [42]. Quaternary and lower Cretaceous deposits of glaciofluvial, aeolian and lacustrine origin cover a large area around the lake [39]. Most deposits are characterized by silt, fine sand and clayey fine sand [43,44].

Table 1 shows the (chrono-)stratigraphy of the Nam Co catchment. The regional stratigraphy consists of the Zhanongtang and Ganmanong formation, both belonging to the Nam Co group as stratigraphic unit. The formations are associated to the upper Pleistocene to Holocene. The older Ganmanong formation, formed between 128 and 12 thousand years b.p., has an average thickness of around 14 m overlain by the younger 3 m thick Zhanongtang formation, formed since 12 thousand years b.p.

Table 1. Lithological and hydrostratigraphic unit of the Nam Co catchment (adapted after [45]).

Chronostratigraphy		Thousand Years Ago (Ka B.P.)	Stratigraphic Unit		Depth	Thickness	Hydrostratigraphic Unit
Period	Series		Nam Co Area		[m]	[m]	
Quarternary	Holocence	4 12	Nam Co Group	Zhanongtang formation	0–3	3	Zhanongtang–Ganmanong aquifer
	Upper Pleistocence	32 40 128		Ganmanong formation	3–17	14	

The Zhagu subcatchment (A = 46 km^2) (Figure 1c) is located at the northeast shoreline of the Nam Co Lake. The subcatchment elevation ranges from 4730 m above sea level (m a.s.l.) at the Nam Co Lake lakeshore located to the west from the catchment valley, to more than 5200 m a.s.l. in the east. Three first-order streams are flowing through the subcatchment, where two first-order streams are merging into a second-order stream. Those streams are infiltrating inside the subcatchment and are therefore surficially disconnected from the Nam Co Lake. Existent stream beds suggest that due to heavy summer monsoon, episodic drainage events might occur into the lake. Due to the absence of glaciers, precipitation is the only source for groundwater recharge. According to the National Geological Archives of China, the valley in the study area (Figure 1c) consists of lacustrine sediments, fluvial sediments and alluvial-proluvial sediments, wherein the mountainous area most likely includes tuff and, to some extent, granite. A terrace geomorphologically divides the catchment into two areas: a lower area in the west facing the Nam Co Lake and a higher valley in the east surrounded by a mountain range.

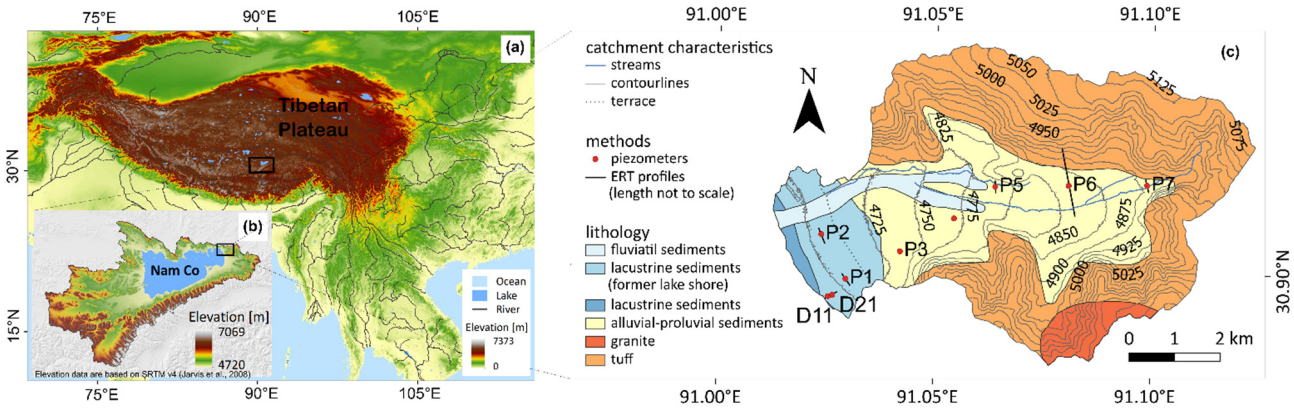

Figure 1. Overview of the study area. (**a**) The topography of the Tibetan Plateau (TP) [46,47], (**b**) second largest lake on the TP: the Nam Co Lake [6], (**c**) lithology and contour lines of the Zhagu subcatchment study area (modified after [45]).

2.2. Hydrogeological, Geophysical, Lithological Analyses

For the hydrostratigraphic characterization (goal I of the present study) and the assessment of the hydraulic conductivity distribution (goal II), the following methods were applied during three field work campaigns (June/July 2018, May 2019 and September 2019): (Section 2.2.1) installation of piezometers, (Section 2.2.2) measurement of depth-to-water-table, (Section 2.2.3) performance of hydraulic field experiments (short pumping tests and slug tests), (Section 2.2.4) analyzing grain size distribution of collected sediment samples, (Section 2.2.5) applying empirical methods to estimate hydraulic conductivity based on grain size distribution ([48,49]), and (Section 2.2.6) recording and analysis of ERT profiles to delineate regional hydrogeological units.

2.2.1. Installation of Piezometers

Nine piezometers with a cumulative piezometer length of 96.5 m were installed during the first field work campaign in June/July 2018. Almost all piezometers are aligned west–east along a dirt road (Figure 1c). Due to the complete lack of subsurface and groundwater table information, the drilling company drilled until wet sediment was reached. To ensure that the piezometers are hydraulically connected to the shallow aquifer, an additional 1 m was drilled. Two piezometers (D11, D21) out of nine were installed near the lake shore. These piezometers were located at a distance of 100 m and 200 m from the lakeshore, respectively. The other 7 piezometers (P1–P7) out of 9 were placed near the dirt road further away from the lakeshore.

The installed piezometers consist of several PVC pipes of 1 m length and outside/inside diameter of 58/50 mm. Prior to installation, the PVC pipes were screwed together, with a manually perforated filter of length L_{BL} = 1.2 m at the lower end. The installed piezometers were closed with caps and covered with boulders for protection against vandalism. The overall length of the piezometers ranged between minimum 4 m (D11) and maximum 15 m (P4).

2.2.2. Measurement of the Depth to Water Table

The depth to water table was measured with an electric contact gauge (Heron instruments Inc., Dundas, ON, Canada) that also measures electric conductivity and temperature. The measurements were taken once in each installed piezometer between the 12 and 15 of May 2019).

2.2.3. Performance of Hydraulic Field Experiments (Short Pumping Tests and Slug Tests)

In September 2019, short pumping tests [50] followed by slug tests [51] were carried out to estimate hydraulic conductivity. Data loggers (dipperLog NANO C 30 m, Heron instruments Inc., Dundas, ON, Canada) were placed 0.5 m above each piezometer bot-

tom to ensure that the logger was placed within the groundwater of the shallow aquifer. Groundwater pressure was continuously logged at a rate of 5 s with an accuracy of 0.1% for short pumping tests and slug tests. The logger internally converts the logged pressure into pressure head using freshwater density of 1000 kg m^{-3}. Pumped water was stored in canisters for use as 'slug' in the subsequent slug tests.

In total, 45 short pumping tests were carried out in 6 piezometers (D11, D21, P2, P5, P6, P7). Multiple short pumping tests were used to reduce the errors of the estimated K values. A groundwater sampling pump (12 V Sampling Pump Super twister 25 mt, ENVIEQ, Tallinn, Estonia) was placed completely in water above the data logger and the piezometer was pumped empty (until no further water was produced).

Figure 2a illustrates the procedure to estimate hydraulic conductivity using the result of a short pumping test. In the figure, Ψ denotes pressure head, Ψ_0 is the original (equilibrium) pressure head, Ψ_1 and Ψ_2 are pressure heads on the recovery curve at times t_1 and t_2, respectively, and $\Delta H_p = \Psi_0 - \Psi_1$, $\Delta h_p = \Psi_0 - \Psi_2$, $\Delta t = t_2 - t_1$. The pressure head Ψ_1 was selected to ensure that the filter length L_{BL} be always fully saturated such that groundwater inflow occurred over the entire filter length. Due to the pressure head gradient induced by pumping, water flows from the aquifer formation back into the piezometer until recovery to the original pressure head Ψ_0. The hydraulic conductivity was estimated by the following equation [50]:

$$K = \frac{r_{BL}^2}{2 \cdot L_{BL} \cdot \Delta t} \cdot 5.3 \cdot \log\left(\frac{L_{BL}}{r_{BL}}\right) \cdot \log\left(\frac{\Delta H_p}{\Delta h_p}\right), \quad (1)$$

where K [m s^{-1}] is hydraulic conductivity, r_{BL} [m] is piezometer radius, L_{BL} [m] is filter length. Equation (1) holds for $\frac{L_{BL}}{r_{BL}} > 8$ [50], which is fulfilled for all the piezometers.

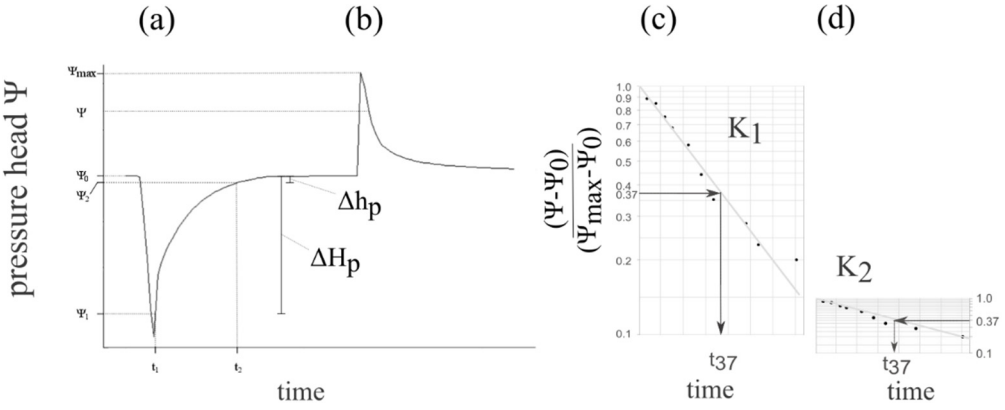

Figure 2. Illustration of the procedure to recover the hydraulic field from field experiments: (**a**) short pumping test recovery curve, (**b**) slug response curve, (**c**) semi-logarithmic slug response curve to assess hydraulic conductivity K1, (**d**) semi-logarithmic slug response curve to assess hydraulic conductivity K2 (modified after Domenico and Schwartz (1998)).

In total, 16 slug tests in all 9 piezometers were carried out. Multiple slug tests reduce measurement errors. The slug tests started by noting the original pressure head Ψ_0 (Figure 2b). The slug was created by instantaneously filling up the piezometer with previously collected water during the short pumping tests, such that Ψ_{max} was the maximum pressure head (Figure 2b). The ratio $\frac{\Psi - \Psi_0}{\Psi_{max} - \Psi_0}$ was semi-logarithmically plotted against time (Figure 2c), t_{37} was read from the plot, and the hydraulic conductivity was estimated after [51]:

$$K = \frac{r_{BL}^2 \ln\left(\frac{L_{BL}}{R}\right)}{2 \cdot L_{BL} \cdot t_{37}}, \quad (2)$$

where t_{37} [s] is the time at which the water level has dropped to 37% of the initial slug signal. In some cases, the semi-logarithmically plotted ratio $\frac{\Psi - \Psi_0}{\Psi_{max} - \Psi_0}$ showed sudden changes in slope (Figure 2c,d). If this happened, the data were separated into different datasets, one

sub-data set for each slope. For each sub-data set, hydraulic conductivity was estimated as per Equation (2), such that a single slug test could lead to multiple K values, denoted K_1 and K_2 in Figure 2.

2.2.4. Analysis of Grain Size Distribution of Collected Sediment Samples

A total of 82 sediment cores from all 9 drilled piezometer boreholes were obtained in June and July 2018 to assess hydrogeological properties at different depths. Cylindrical samples (d = 5 cm, h = 8 cm) were taken during drilling when sediment texture or color changed. The samples were air-dried and grain size analyses were conducted according to the procedure used by [52]. In order to represent original subsurface flow characteristics, organic matter and Fe-oxides were retained. The definitions of textural classes and sand subclasses were based on FAO Guidelines for Soil Description [53].

2.2.5. Estimation of the Hydraulic Conductivity based on Grain Size Distribution

Hydraulic conductivity can be estimated from grain size distribution using empirical relationships. In the Excel-based tool HydroGeoSieveXL [54], 15 empirical models are implemented that read grain size distribution in order to estimate a hydraulic conductivity value associated to the read grain size distribution. After reading grain size distribution, HydroGeoSieveXL examines applicability of all 15 methods to that grain size distribution. For the samples taken in the present study, HydroGeoSieveXL determined that the two models of [48,49] were applicable for all samples. These two models differ in the choice of N and d_e (Table 2), while for both models the hydraulic conductivity was calculated according to [54]:

$$K = \frac{\rho g}{\mu} N \phi(n) d_e^2, \quad (3)$$

where K (m s^{-1}) is hydraulic conductivity, ρ (kg m^{-3}) is temperature-dependent water density, g (m s^{-2}) is gravitational constant, μ (kg m^{-1} s^{-1}) is dynamic viscosity of water, N (−) is a constant shape factor dependent on the model, $n = 0.255 \cdot \left(1 + 0.83^{U}\right)$ (−) is porosity, $U = \frac{d_{60}}{d_{10}}$ (−) is unconformity coefficient, $\phi(n) = \frac{n^3}{(1-n)^2}$ (−) is a porosity function, d_e (e = 10 or 17) (m) is an effective grain size of the grain size distribution.

To estimate hydraulic conductivity using the two models, 2–4 samples were taken at different depth in 8 piezometers (D11, D21, P1, P2, P4, P5, P6, P7), giving a total of 26 aquifer sediment samples. The samples were located below the measured water level to ensure that aquifer material was sampled.

Table 2. Overview of selected empirical mathematical models to estimate hydraulic conductivity K (modified after [54]).

Source	N	d_e	Applicable Conditions
Vukovic and Soro (1992)	$\left(3.75 \cdot 10^{-5}\right) \cdot \tau$ $\tau 1.093 \cdot 10^{-4} T^2 + 2.102 \cdot 10^{-2} T + 0.5889$	d_{17}	sand and sandy clay $d_{10} < 0.05$ cm
Barr (2001)	$\frac{1}{(36) \cdot 5 C_s^2}$	d_{10}	unspecified

N = constant dependent on characteristics of the porous medium
T = water temperature (°C)
$C_s^2 = 1$ for spherical grains
d_{10} = grain size (cm) corresponding to 10% by weight passing through the sieves
d_{17} = grain size (cm) corresponding to 17% by weight passing through the sieves

2.2.6. Recording and Analysis of ERT Profiles

In order to assess the water saturation and to eventually identify a shallow aquifer, 7 electrical resistivity tomography (ERT) profiles were recorded along previously installed piezometers (except P3 and P4). To obtain a subsurficial representation of water saturation and of a regional hydrostratigraphic unit, 5 parallel ERT profiles (along piezometers P1, P2, P5, P6, P7) were aligned north–south. In addition, two more profiles near the lake (along piezometers D11, D21) were aligned west–east.

In the ERT, a spatial section of the resistivity of the subsurface is obtained by combining multiple 4-point measurements. Each 4-point measurement requires two electrodes to inject current, and two electrodes to measure the voltage. An apparent resistivity value is obtained from the ratio between voltage and current by multiplication with a geometry factor which depends on the electrode configuration. Here, the Wenner configuration [55] was used, where all distances between neighboring electrodes are identical. The two outer electrodes inject current, and the two inner electrodes measure the voltage [55].

In order to acquire multiple 4-point measurements necessary to obtain a spatial resistivity distribution along a profile vs. depth, the multi-electrode equipment "GeoTom-MK" (GEOLOG2000, Augsburg, Germany) with 50 electrodes was used. For each single measurement, 4 of the 50 electrodes are used in a Wenner configuration, and all possible 4-point measurements are then taken to obtain a full coverage of the subsurface.

The profile length (PL) constrains the maximum electrode spacing (i.e., the maximum possible distance between the current electrodes), which controls the maximum depth of investigation (DOI). Since there is no fixed relationship between profile length and DOI, a rule of thumb was used (DOI = 0.2 PL; [56]. For each piezometer location, the piezometer depth was used to fix the desired DOI and thus the profile length. The spacing between the neighboring electrodes was then adjusted to obtain the desired profile lengths. This resulted in PL varying between 14 m and 98 m. Profile P6 constitutes an exception to this procedure. Its total length is 1196 m, and it is composed of overlapping sub-profiles using a roll-along procedure described in Buckel et al. (2020). In order to convert the measured apparent resistivity data into 2D resistivity models of the subsurface, data were inverted using the inversion software RES2Dinv [57].

The resistivity of sediment can be calculated using the empirical formula developed by [58], defined as:

$$R_{arc} = an^{-m}s^{-n_s}R_w, \quad (4)$$

where R_{arc} (Ωm) is bulk electrical resistivity of the subsurface, a (−) is tortuosity factor, ranging between 0.5 and 1.5 [59], m (−) is cementation factor, ranging between 1.3 and 2.6 [59], s (−) is fraction of pores filled with fluid, n_s (−) is saturation exponent, which is typically 2, R_w (Ωm) is electrical resistivity of the pore water.

Archie's law calculates the bulk electrical resistivity of the subsurface R_{arc} based on porosity n, electrical conductivity of pore water σ_w measured in situ, and the fraction of pores filled with fluids [55]. Based on grain size analyses (details in Section 3.2 Sediment profile results), it is assumed here that no significant clay content is present in the sandy aquifer material such that Archie's law of 1942 is valid [60]. It indicates that bulk electrical resistivity of the subsurface decreases with increasing water content.

With the assumption of saturated unconsolidated sandy aquifer material, the appropriate parameter values in Archie's law are [55]: s = 1, a = 1 and m = 1.3. The porosity n was calculated based on grain size distribution using $n = 0.255 \cdot \left(1 + 0.83^{U}\right)$ [48] and $U = \frac{d_{60}}{d_{10}}$ [54], while electrical conductivity σ_w was measured in situ (Appendix A, Table A1). During the second field work campaign in May 2019, a measurement of electrical conductivity of groundwater was taken once in each piezometer (D11, D21, P1, P2, P5, P6, P7), where ERT profiles were available, using a conductivity device (Heron instruments Inc., Dundas, Canada). Afterwards, σ_w was converted into electrical resistivity R_w with $R_w = \frac{1}{\sigma_w}$.

3. Results

3.1. Depth-to-Water-Table Results

The depth to water table was measured in 8 out of 9 piezometers (D11, D21, P1, P2, P, P6, P7; Figures 3B and 4B). The four piezometers located close to surface water bodies (D11, D21 near Nam Co Lake, and P5, P7 in the valley near streams; Figure 1) showed small depths to water table, varying between 1 m (D11) and 3 m (P7) (Figures 3B(a) and 4B(c)). This points to the existence of shallow surface water bodies, indicating possible surface–subsurface hydraulic interaction. In contrast, the four piezometers away from surface water bodies (piezometers P1, P2 are located east of D11 and D21; piezometers P4, P6 are located in the valley zone; Figure 1) revealed larger depth to water table, varying between 5.75 m (P1) and 8.06 m (P4) (Figures 3B(a) and 5). This observation indicates no or no significant surface–subsurface hydraulic interaction at around 6–8 m depth. These measurements suggest the existence of a local shallow aquifer whose top range is between 1 m and 8 m below ground surface.

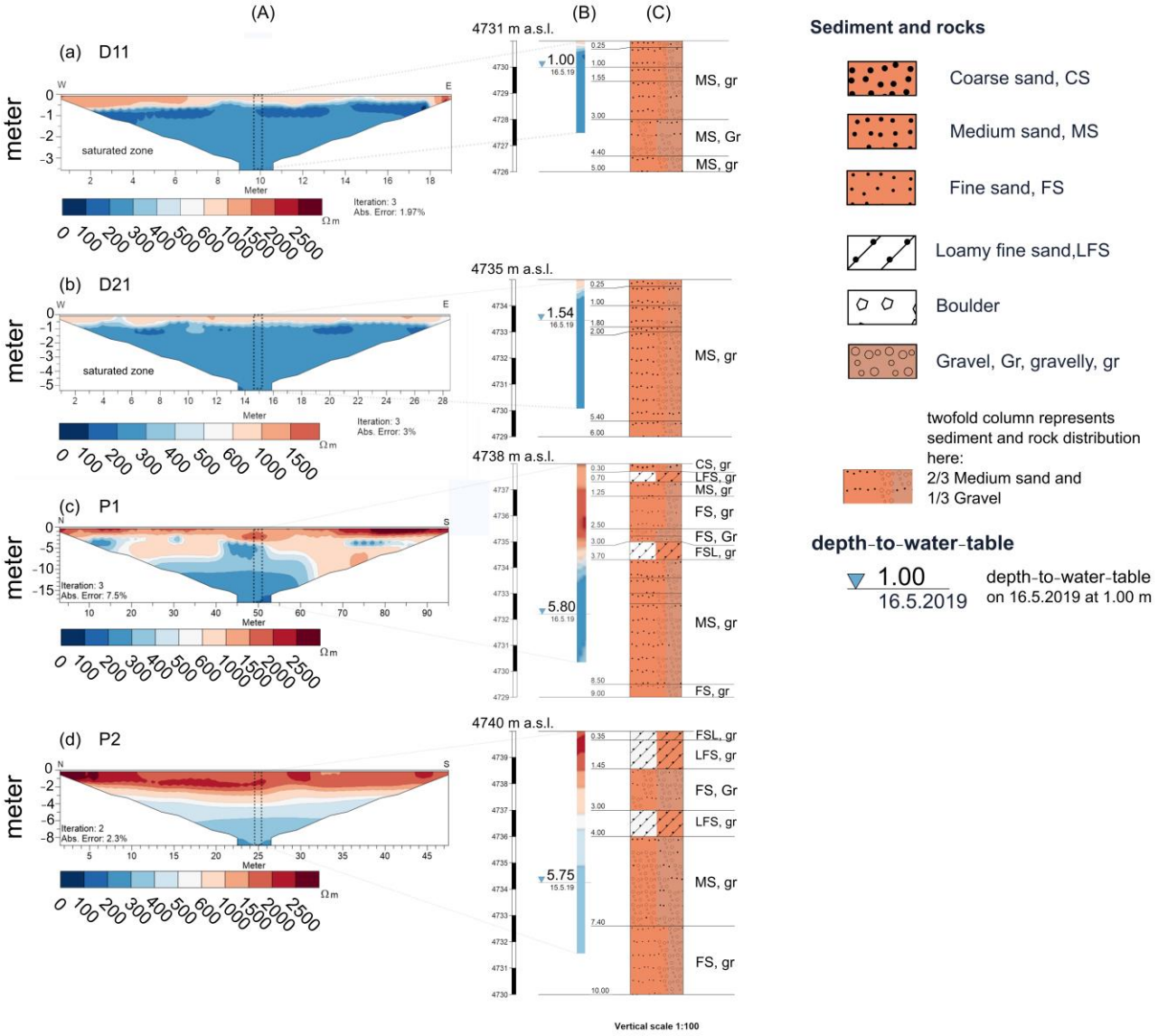

Figure 3. Integration of (**A**) electrical resistivity tomography (ERT) profiles, (**B**) selected column of the ERT profile at the piezometer location near the lake shore and (**C**) sediment profiles of site D11, D21, P1 and P2 with depth-to-water-table measurements. Electrical resistivity values below 500 Ωm were interpreted as saturated zones, which was confirmed by depth-to-water-table measurements. (**a**), (**b**), (**c**) and (**d**) refer to piezometers D11, D21, P1 and P2.

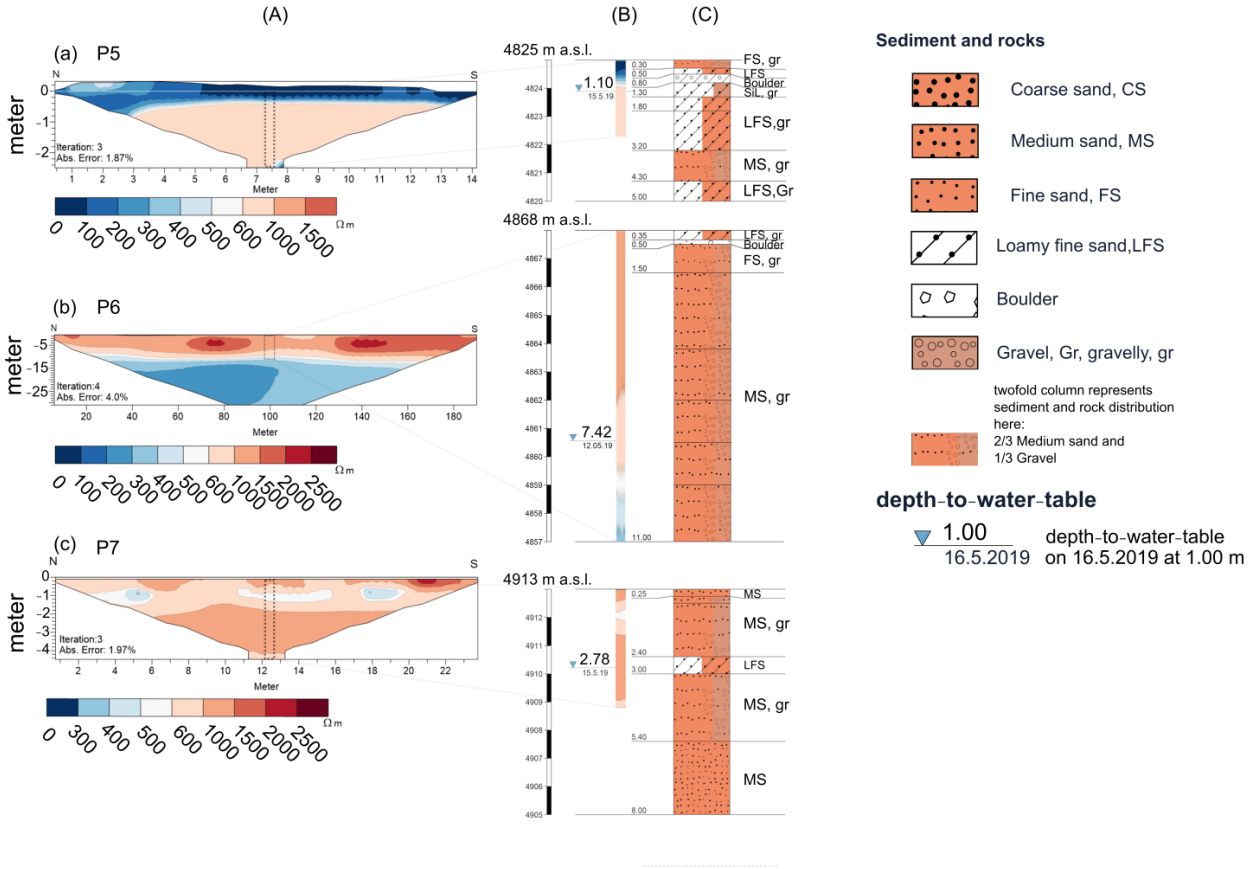

Figure 4. Integration of (**A**) electrical resistivity tomography (ERT) profiles, (**B**) selected column of the ERT profile at the piezometer location in the valley and (**C**) sediment profiles of site P5, P6 and P7 with depth-to-water table measurements. Electrical resistivity values below 500 Ωm were interpreted as saturated zones proved by depth-to-water-table measurements. (**a**), (**b**) and (**c**) refer to piezometers P5, P6 and P7.

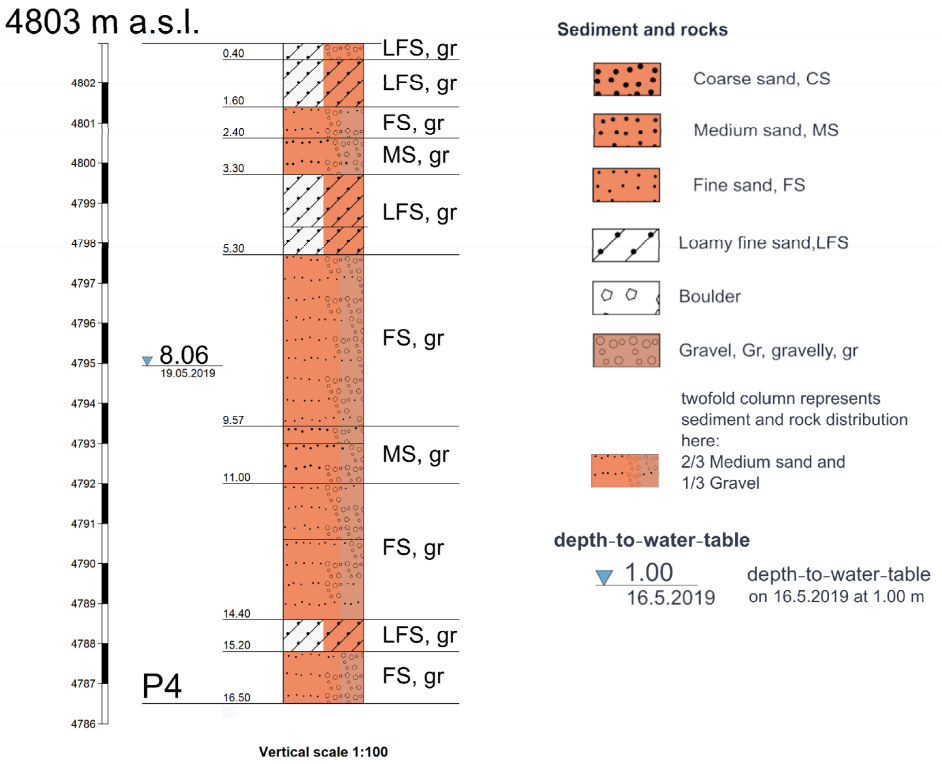

Figure 5. Sediment profile of site P4 with depth-to-water-table measurement.

3.2. Sediment Profile Results

Figures 3C, 4C and 5 present sediment profiles based on grain size analysis for piezometers near the lake shore (D11, D21, P1, P2) and for piezometers in the valley (P4, P5, P6, P7). Grain size analysis of profiles D11 and D21 revealed over 85% medium sand (MS) in both profiles over the entire depth, such that the existence of confining layers can be excluded. This result suggests that the aquifer is unconfined. The material in the analyzed profiles is largely homogeneous over depth and represents the aquifer material. The sediment composition of profiles P1 and P2 until the depth of 5 m (20% silt and clay, 80% fine sand (FS) and medium sand (MS)) can be classified as loamy fine sand (LFS) according to the FAO Guidelines [53]. This result correlates with findings from [44], who studied two profiles from the Nam Co Lake terrace, showing sandy loam and silt until 2 m depth. In the present study, the sediment composition changes to more than 90% FS and MS below 5 m depth, such that the material at P1 and P2 is, in principle, heterogeneous over depth. However, the groundwater level at P1 and P2 was measured to be around 5 m depth, such that the aquifer material found below 5 m depth can be regarded as homogeneous over depth.

Sediment profiles along with depth-to-water-table measurements revealed that some profiles may be heterogeneous over depth, while the material in the aquifer zone is mostly homogeneous over depth, and consists of unconsolidated sandy aquifer material, with fine to medium sand in P4, loamy fine sand to medium sand in P5, and medium sand in P6 and P7 (Figures 4C and 5). The results compare very well with those of [61], who examined the development of soil in the Nam Co catchment close to the Zhagu subcatchment and demonstrated that soil near the ground surface (max. 180 cm) mainly consists of sand (91%). The present study further demonstrates that sediment profiles near the lake differ from those located in the valley, indicating that the aquifer is laterally heterogeneous and homogeneous over depth.

3.3. Empirical Hydraulic Conductivity Results

Empirical mathematical equations are used to estimate K in order to strengthen the understanding of aquifer heterogeneity by presenting actual K values. Figure 6c,d shows estimated K values using the empirical equations of (c) [48] and (d) [49] based on previously conducted grain size analyses (Section 3.2) for piezometers D11, D21, P1, P2, P4, P5, P6, P7. Both methods estimate comparable K values of profiles in all piezometers. Estimated K values tend to be large near the lake shore (10^{-5} m s^{-1} to 10^{-4} m s^{-1}), while smaller K ranges are found in the valley (10^{-6} m s^{-1} to 10^{-5} m s^{-1}). The results indicate the existence of two hydraulic conductivity zones. Therefore, K values estimated by empirical equations support the finding from Section 3.2 that the aquifer is laterally heterogeneous, where a K value within a range of uncertainty can be assigned to each piezometer location in the regional aquifer.

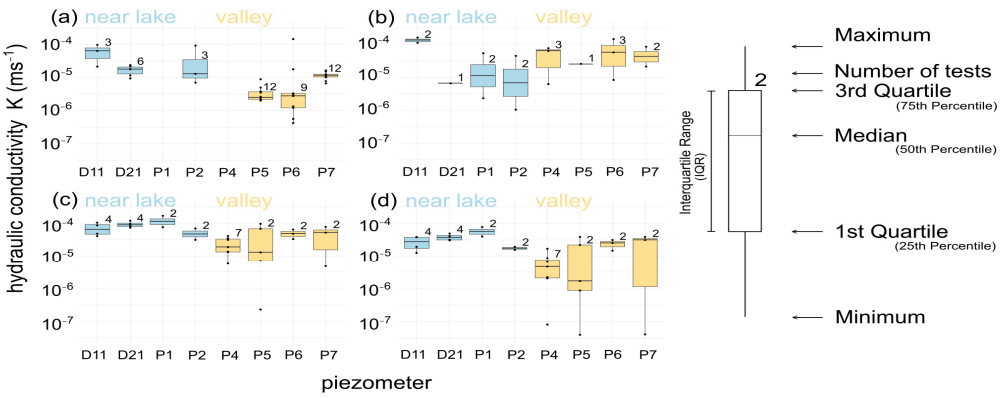

Figure 6. Results of hydraulic conductivity estimation: (**a**) short pumping test, (**b**) slug test, (**c**) based on Vukovic and Soro (1992) and (**d**) based on Barr (2001). Blue coloration denotes piezometers near lake shore and yellow coloration refers to piezometers in the valley.

3.4. Hydraulic Field Experiments (Short Pumping Tests and Slug Tests)

Field tests (short pumping tests and slug tests) were partially conducted for redundancy but mainly to further increase the reliability of K values estimated by empirical equations. Figure 6 shows estimated hydraulic conductivities (K) for eight piezometers D11, D21, P1, P2, P4, P5, P6, P7 based on (a) short pumping tests and (b) slug tests. Both tests show similar hydraulic conductivity values ranging between 10^{-7} m s^{-1} and 10^{-4} m s^{-1}.

Figure 6a presents K values estimated from short pumping tests showing that K varies in space. Most piezometers located at the lake shore (D11, D21, P2) show K values ranging between 10^{-5} m s^{-1} and 10^{-4} m s^{-1}, while piezometers located in the valley (P5, P6, P7) showed smaller K values ranging between 10^{-7} m s^{-1} and 10^{-5} m s^{-1}, such that the estimated K values reveal two different K groups: larger K values at the lake shore and smaller K values in the valley. Figure 6b shows K values estimated from slug tests. A spatial variation in K was also observed here. Piezometer D11, located at 100 m distance from the Nam Co Lake, had the highest K values of 10^{-4} m s^{-1}, while the other piezometers D21, P1, P2, P4, P5, P6, P7 showed smaller ones between 10^{-6} m s^{-1} to 10^{-5} m s^{-1}. Both hydraulic field tests suggest spatial K variation: K values found near the lake shore (10^{-5} m s^{-1} to 10^{-4} m s^{-1}) are larger than those identified in the valley (10^{-7} m s^{-1} to 10^{-5} m s^{-1}). The K ranges associated to both zones are in good agreement with those found by empirical methods in Section 3.3. Empirical equations and hydraulic and field experiments confirm that the aquifer is laterally heterogeneous, and homogeneous over depth. The aquifer can therefore be regarded as an unconfined two-dimensional heterogeneous system whose spatial K zonation can be restrained as per the results presented in the following Section 3.5.

3.5. Regional Hydraulic Conductivity Distribution

Figure 1c presents the lithological map with fluvial and lacustrine sediments at the lake shore, where alluvial-proluvial sediments are dominant inside the valley. Fluvial and lacustrine deposits can contain sandy to clayey grain sizes [62], resulting in relatively large hydraulic conductivity ranges. This coincides with lithology and K values of two K-zones as measured in the present study.

The lithological map (Figure 1) suggests existence of a third K-zone located in the mountain range consisting of mainly tuff [45]. Hydraulic conductivity of tuff can vary by several orders of magnitude due to very different genesis where tuff formation is strongly dependent on the formation processes [63]. Because the mountain range in the study area is extremely difficult to access, hydraulic field tests could not be carried out there, such that other studies related to K values of tuff were considered. Appel and Habler (2002) assessed two sites with regional tuff in Sellafield (Great Britain) and Yucca Mountain (NV, USA). For hydraulic conductivity estimation, 260 single-borehole packer tests were conducted, resulting in large ranges of K values. The K values found in the tuff in Sellafield showed the large range of 10^{-16} to 10^{-7} m s^{-1}, which was even larger for the tuff located at Yucca Mountain (10^{-16} to 10^{-4} m s^{-1}). The mean K values identified at these sites were 10^{-12} m s^{-1} and 10^{-7} m s^{-1}, respectively. In the complete absence of prior field studies and field test results in the tuff formation of the subcatchment regarded here, a third K-zone is established whose K value is assumed to range between 10^{-12} to 10^{-7} m s^{-1}, adopted from the mean K values found by Appel and Habler (2002). Based on short pumping tests, slug tests, empirical mathematical methods and assumed K values for tuff from Appel and Habler (2002), it is assumed that the study area consists of 3 K-zones with given K ranges: K-zone 1 (10^{-5} to 10^{-4} m s^{-1}), K-zone 2 (10^{-7} to 10^{-5} m s^{-1}) and K-zone 3 (10^{-12} to 10^{-7} m s^{-1}) (Figure 7).

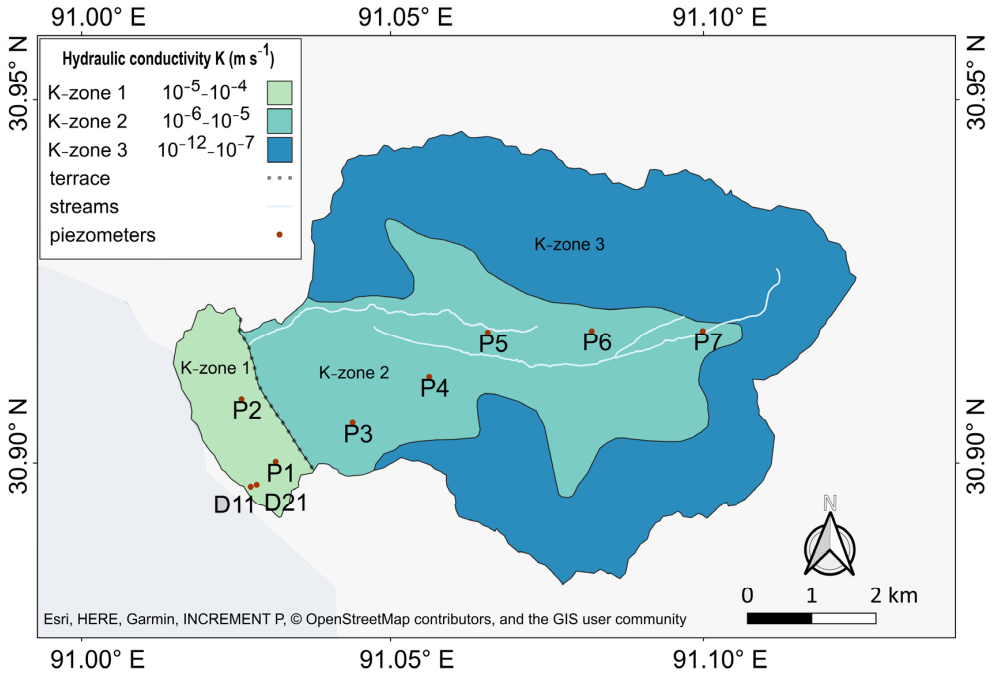

Figure 7. Lithological map with estimated hydraulic conductivity ranges based on field tests and empirical mathematical models.

3.6. Electrical Resistivity Tomography Results and Archie's Law

A total of seven vertical 2D electrical resistivity tomography (ERT) profiles were recorded in order to get a subsurficial picture of water saturation and of regional hydrostratigraphic units of the Zhagu subcatchment. According to [64], fresh water typically has electrical resistivity value below 100 Ωm, while unsaturated gravel and sand have electrical resistivity values larger than 800 Ωm, and permafrost shows values between 1000 Ωm and 100,000 Ωm. Water is a good electrical conductor, therefore saturated sand will have a resistivity value below 800 Ωm due to water-filled pores. [65] stated that electrical resistivity values near the ground surface with values below 700 Ωm indicate the presence of a saturated zone. It is therefore assumed here that the regional aquifer can be identified by electrical resistivity values below 500 Ωm.

The ERT profiles at D11, D21, P1, P2 located near the lake shore indicate two electrical conductivity zones with high electrical resistivity values (500 Ωm to more than 2500 Ωm) near the ground surface and low electrical resistivity values (below 500 Ωm) at larger depth. This suggests the presence of unsaturated sediments near the ground surface and saturated sediments at larger depth. The ERT profiles at D11 and D21 show a shift from high electrical resistivity values (unsaturated zone; 500 Ωm to more than 2500 Ωm) to low electrical resistivity values (saturated zone; below 500 Ωm) in around 40 cm to 50 cm depth, while profiles at P1, P2 and P6 (Figure 3A) reveal that the change from unsaturated to saturated conditions is at approximately 4 m, 5 m, and 11 m depth, respectively. Figure 4A presents ERT profiles at P5 and P7 (in the valley) with low electrical resistivity below 500 Ωm and 500 Ωm to 1000 Ωm, respectively, near the ground surface (maximum 2 m depth), indicating high to moderate saturation near the ground surface. This saturation might be related to recent monsoonal activities. At greater depths, higher electrical resistivities between 1000 Ωm to 100,000 Ωm were not detected, indicating the absence of permafrost at the locations of both piezometers. This was also observed at piezometer locations D11, D21, P1, P2, P6.

Archie's law was applied for piezometers D11, D21, P1, P2, P5, P6, P7 to calculate bulk electrical resistivity values that are related to the regional aquifer by using in situ measured electrical conductivity of formation water. The values were calculated with porosities determined from grain size analyses below the groundwater table, assuming

full water saturation ($s = 1$). The in situ measured electrical conductivity of formation water showed overall values between 0.02 and 0.09 S m^{-1}, corresponding to resistivity values between 11 and 50 Ωm. These low resistivity values reveal a significant amount of dissolved solids in the regional groundwater. The calculated bulk electrical resistivity values agree with the in situ measured resistivity values for piezometers D11, D21, P1, P2, P5, P6, P7 and show values below 200 Ωm (Appendix A, Table A1). Those resistivity values were then compared to electrical resistivity values determined by ERT below the water table, showing that the bulk electrical resistivity values gained by Archie's law are in good agreement with electrical resistivity values previously obtained from the ERT profiles. The agreement supports the assumptions that a regional but potentially contaminant aquifer is present, and that the regional aquifer can be identified by electrical resistivity values below 500 Ωm.

3.7. Regional Hydrostratigraphy

Each of the applied hydrogeophysical and mathematical methods provides piece-wise details of the hydrogeology in the Zhagu subcatchment. Integrating and combining results of all methods provides an overall insight and subsurficial picture of the hydrostratigraphy and of the regional hydrogeology of the found aquifer. The initially carried out depth-to-water-table measurements revealed presence of an aquifer at 1 m to 8 m depth below ground surface. Detailed sediment profiles based on grain size analyses further indicated that the sandy aquifer is laterally heterogeneous and homogeneous over depth. Estimates of hydraulic conductivity from both empirical mathematical equations ([48,49]) and from field tests (short pumping tests, slug tests) further confirmed aquifer heterogeneity, and constrain the hydraulic conductivity values in the lithology distribution of the study area (Figure 1). Combination of the lithology and estimated K values lead to an assumed existence of three hydraulic conductivity zones within the study area. The ERT profiles confirmed the existence of the regional aquifer, and provided a spatial picture from selected points of the aquifer (Figure 8).

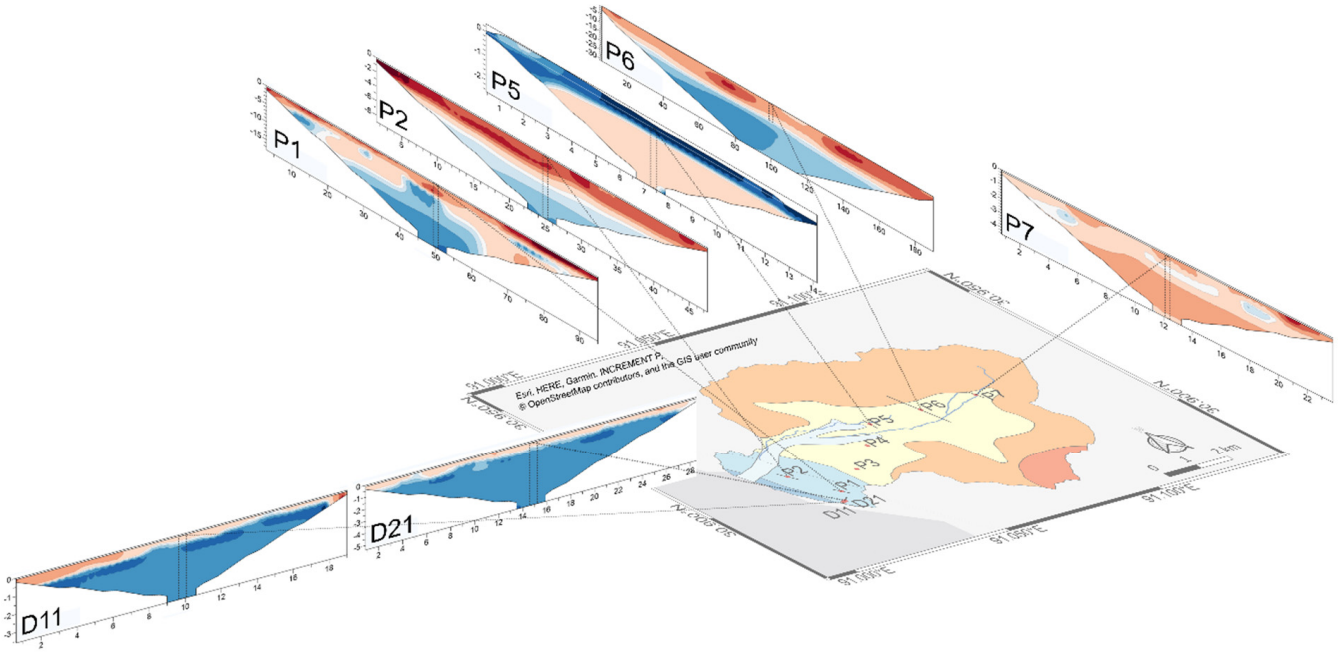

Figure 8. Spatial picture of the Zhagu subcatchment with the ERT profiles. Color coding of the ERT images is identical to that used in Figures 3 and 4.

Table 1 shows stratigraphic units of the Nam Co catchment, consisting of the older Ganmanong formation and the younger Zhanongtang formation. According to the Development Research Center of China (2020) the Ganmanong formation is related to the upper Pleistocene, having a thickness of 14 m. During the Holocene, the Ganmanong formation was overlain by the Zhanongtang formation with a thickness of 3 m, showing that the entire Quaternary formation has a total thickness of 17 m. The deepest recorded sediment profile of 11 m and the deepest ERT profile of 30 m were measured in P6 (Figure 4B(a),(c)), while all other sediment profiles and ERT profiles were less deep than 17 m. Therefore, all analyses conducted in this study are located either within the Zhanongtang formation or the Ganmanong formation (Table 1). According to [66], a hydrostratigraphic unit consists of a formation or a group of formations with similar hydrologic characteristics, allowing grouping into an aquifer. Therefore, the two Quaternary formations analyzed in this study can be grouped into a single hydrostratigraphic unit, which is hereby named the Zhanongtang–Ganmanong aquifer.

4. Discussion

4.1. Hydrostratigraphic Unit

Our study shows that the delineated aquifer formation can be classified as a Quaternary hydrostratigraphic unit. The aquifer is interpreted as unconfined and shallow Zhanongtang–Ganmanong aquifer. The identified Zhanongtang–Ganmanong aquifer mainly consists of unconsolidated sandy material, which is in agreement with results by Lehmkuhl et al. (2002), who examined soil in the Nam Co catchment close to the Zhagu subcatchment and revealed that soil near the ground surface mainly consists of 91% sand.

Sediment near the lake has been influenced by former higher lake water levels that formed well-mixed lake sediments, resulting in homogeneous sediment profiles near the lake. In contrast, sediments in the valley are of alluvial, fluvial or glacial origin, which typically results in heterogeneous material as confirmed by the profile analyses carried out here. The field investigations indicated presence of boulders forming lines near the valley borders, which was interpreted as lateral moraine deposits. This provides evidence that sediments in the first 5 m have likely been transported by glaciers during the Holocene. Glacial activity in the valley also explains the loamy fine sand texture (LFS), which is a distinctive component of glacial till that is assumed to have been transported below and in front of the former glacier forming ground moraine and end moraine, respectively.

According to [20], the TP is the primary permafrost zone in China and the Nam Co catchment is located in a sporadic permafrost zone, which means that isolated permafrost patches are present in the Nam Co catchment. Based on the sediment analyses and ERT results presented here, permafrost patches could not be identified to a depth of 17 m for piezometers located between 4730 m a.s.l. and 5200 m a.s.l. In conclusion, permafrost can be assumed to be absent in the Zhagu subcatchment. This finding is in line with results by [67], who expect presence of permafrost above an elevation of 5300 m a.s.l. along the northern slope of the Mount Nyainqentanglha, south of the Nam Co Lake.

4.2. Hydraulic Conductivity Distribution

Our results show that the study area consists of three K-zones, showing different K ranges between 10^{-12} m s^{-1} and 10^{-4} m s^{-1}. A given number of locations where field tests were conducted does not reflect the exact hydraulic conductivity distribution in the study area. However, when combining the lithological map provided by [45]. Development Research Center of China (2020) with the estimated K values at the piezometer locations, the gained K-zonation is assumed to be a realistic representation of the true K distribution. Refs. [68,69] applied in situ experiments along the Qinghai–Tibet Railway (Golmud–Anduo) and showed that K values range from 10^{-8} to 10^{-4} m s^{-1}, which is a similarly large K range to the one found in the present study. Therefore, it is further shown here that estimated K values are comparable with those from previous studies conducted on the Tibetan Plateau.

4.3. Knowledge Transfer of Combined Methods from the Investigated Zhagu Subcatchment

Different hydrogeophysical and lithological methods were applied and combined in the selected Zhagu subcatchment. Other sites of the Nam Co catchment show the same lithology, and it can be assumed that those sediments are of similar genesis. Based on this assumption, K ranges that were found for lithology within the Zhagu subcatchment are also expected in other sites within the Nam Co catchment. Thus, expensive and remote field campaigns consisting of in situ experiments followed by time-intensive laboratory analyses may therefore not be required at sites with the same lithology. For other lithologies (marked in white in Figure 9), installation of piezometers and carrying out field tests are necessary in order to estimate K ranges.

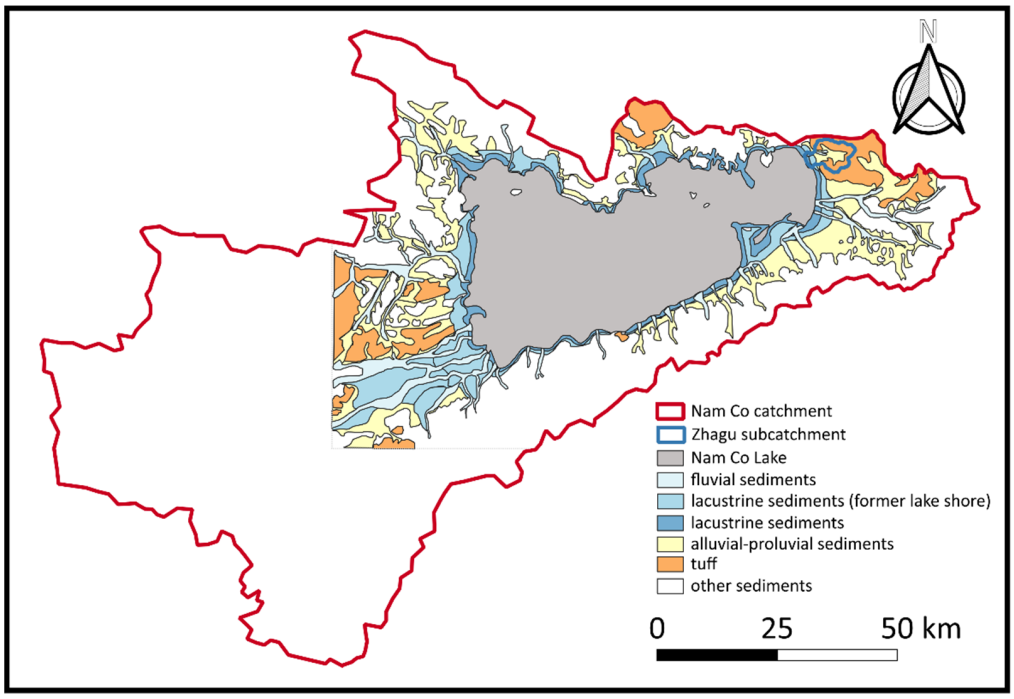

Figure 9. Nam Co catchment lithology (modified after Development Research Center of China (2020)).

5. Summary and Conclusions

This study presents the application of an integrated hydrogeologic, lithological and geophysical approach to the remote and previously ungauged mountainous Zhagu subcatchment on the TP. In contrast to existing hydrological studies in the Nam Co catchment, we used multiple analysis methods to (I) delineate a shallow regional aquifer along with a hydrostratigraphic unit, and to (II) characterize the hydraulic conductivity distribution. The individual results gained by interdisciplinary methods are generally in good agreement. Consequently, the results give combined first insights into hydrogeological conditions in the Nam Co catchment.

In summary, key contributions and new findings of this study are:

(1). The Nam Co catchment consists of a hydrostratigraphic unit, which is named the Zhanongtang–Ganmanong aquifer according to the two identified Quaternary formations. The high mountain aquifer is successfully delineated using well-established methods in low altitudes, and the identified sandy aquifer is found to be shallow, unconfined, laterally heterogeneous and homogeneous over depth.

(2). The Zhagu subcatchment consists of 3 hydraulic conductivity zones, showing large hydraulic conductivity (K) values near the lake (10^{-5} m s^{-1} to 10^{-4} m s^{-1}), small K values in the valley (10^{-6} m s^{-1} to 10^{-5} m s^{-1}), and low K values in the mountain area (10^{-12} m s^{-1} to 10^{-7} m s^{-1}). Detailed application of hydraulic field experiments

followed by laboratory analyses and comparison with a lithological map revealed K ranges for different sediments of the Zhagu subcatchment.

(3). The Zhagu subcatchment currently shows no evidence of permafrost patches between 4730 m a.s.l. and 5200 m a.s.l. This supports the hypothesis of Tian et al. (2009), who stated that permafrost can only be found in elevations above 5300 m a.s.l. at the northern slope of Mt. Nyainqentanglha mountain which is part of the Nam Co catchment.

The achieved results contribute to first hydrogeological insights of the Nam Co catchment. These insights are important for the transferability to other unexplored subcatchments surrounding the Nam Co Lake and elsewhere on the TP where lithology and sediments are similar. This can help to answer scientific questions of future water fluxes, water budgets and climatic change on the TP. Hydrogeological knowledge helps to improve and regulate water management for billions of people in Central Asia. Future work will further include monsoonal influence on groundwater dynamics in the Zhagu subcatchment.

Author Contributions: Conceptualization, T.V.T. and J.B.; data curation, T.V.T. and J.B.; formal analysis, T.V.T.; funding acquisition, A.S., G.G., F.Z., A.H., T.G.; investigation, T.V.T., J.B., P.M., H.T. and Z.Y.; methodology, T.V.T., J.B., P.M., A.H. and A.S.; project administration, T.G.; resources, T.V.T., H.T., Z.Y. and F.Z.; software, T.V.T.; supervision, A.H., F.Z. and T.G.; validation, T.V.T.; visualization, T.V.T.; writing—original draft, T.V.T.; writing—review and editing, T.V.T., J.B., P.M., H.T., Z.Y., A.H., G.G., F.Z., A.S. and T.G. All authors have read and agreed to the published version of the manuscript.

Funding: This research is a contribution to the International Research Training Group "Geo-ecosystems in transition on the Tibetan Plateau (TransTiP), funded by Deutsche Forschungsgemeinschaft (DFG grant 317513741/GRK 2309). The publication of this article was funded by the Open Access Fund of the Leibniz Universität Hannover.

Institutional Review Board Statement: Not applicable.

Informed Consent Statement: Not applicable.

Data Availability Statement: The Tibetan Plateau dataset is available at http://www.geodoi.ac.cn/weben/doi.aspx?Id=135 (accessed 20 May 2020) [43]. The Excel-based tool "HydrogeoSieveXL" used in this study is available at https://kuscholarworks.ku.edu/handle/1808/21763 (accessed 10 January 2019). The soil profiles were created with the "Profil Tec" Software (Version 7.10), available at https://geologik.com/profiltec (accessed 23 November 2018). The SRTM data V4 is available from https://srtm.csi.cgiar.org (accessed 14 April 2021).

Acknowledgments: We thank all colleagues and institutions involved in this study, especially during field work and data collection. We would like to thank the Internation Centre for Trpical Agriculture (CIAT) for providing the SRTM and special thanks go to Eike Reinosch, who helped in constructing the overview map. The constructive comments of three anonymous reviewers are greatly appreciated and have helped improve this manuscript.

Conflicts of Interest: The authors declare no conflict of interest.

Appendix A

Table A1. Overview of in situ measured electrical conductivity σ_w and calculated electrical resistivity R_{arc} based on Archie's Law.

Piezometer	σ_w (S m^{-1})	R_{arc} (Ωm)
D11	0.0197	196.09
D21	0.0318	122.02
P1	0.0294	129.11
P2	0.0304	140.00
P5	0.0922	63.57
P6	0.0445	84.37
P7	0.02886	124.28

References

1. Kang, S.; Xu, Y.; You, Q.; Flügel, W.-A.; Pepin, N.; Yao, T. Review of climate and cryospheric change in the Tibetan Plateau. *Environ. Res. Lett.* **2010**, *5*, 015101. [CrossRef]
2. Xiang, L.; Wang, H.; Steffen, H.; Wu, P.; Jia, L.; Jiang, L.; Shen, Q. Groundwater storage changes in the Tibetan Plateau and adjacent areas revealed from GRACE satellite gravity data. *Earth Planet. Sci. Lett.* **2016**, *449*, 228–239. [CrossRef]
3. Immerzeel, W.W.; Lutz, A.F.; Andrade, M.; Bahl, A.; Biemans, H.; Bolch, T.; Hyde, S.; Brumby, S.; Davies, B.J.; Elmore, A.C.; et al. Importance and vulnerability of the world's water towers. *Nature* **2020**, *577*, 364–369. [CrossRef] [PubMed]
4. Cuo, L.; Zhang, Y.; Zhu, F.; Liang, L. Characteristics and changes of streamflow on the Tibetan Plateau: A review. *J. Hydrol. Reg. Stud.* **2014**, *2*, 49–68. [CrossRef]
5. Anderson, M.P.; Woessner, W.W. *Applied groundwater modeling Simulation of Flow and Advective Transport*; Academic Press: Cambridge, MA, USA, 1992; ISBN 0120594854.
6. Kang, S.; Yi, Y.; Xu, Y.; Xu, B.; Zhang, Y. Water Isotope framework for lake water balance monitoring and modelling in the Nam Co Basin, Tibetan Plateau. *J. Hydrol. Reg. Stud.* **2017**, *12*, 289–302. [CrossRef]
7. Yang, K.; Wang, J.; Lei, Y.; Chen, Y.; Zhu, L.; Ding, B.; Qin, J.; Qin, J. Quantifying evaporation and its decadal change for Lake Nam Co, central Tibetan Plateau. *J. Geophys. Res. Atmos.* **2016**, *121*, 7578–7591. [CrossRef]
8. Zhang, Q.; Kang, S.; Wang, F.; Li, C.; Xu, Y. Major ion geochemistry of Nam Co lake and its sources, Tibetan Plateau. *Aquat. Geochem.* **2008**, *14*, 321–336. [CrossRef]
9. Wu, H.; Wang, N.; Jiang, X.; Guo, Z. Variations in water level and glacier mass balance in Nam Co lake, Nyainqentanglha range, Tibetan Plateau, based on ICESat data for 2003-09. *Ann. Glaciol.* **2014**, *55*, 239–247. [CrossRef]
10. Tong, K.; Su, F.; Xu, B. Quantifying the contribution of glacier meltwater in the expansion of the largest lake in Tibet. *J. Geophys. Res. Atmos.* **2016**, *121*, 1–158. [CrossRef]
11. Zhou, S.; Kang, S.; Chen, F.; Joswiak, D.R. Water balance observations reveal significant subsurface water seepage from Lake Nam Co, south-central Tibetan Plateau. *J. Hydrol.* **2013**, *491*, 89–99. [CrossRef]
12. Du, Y.; Xie, M.W.; Hu, M. Mechanism of Lake Area Variations and Water Level Changes in Nam Co Lake. *Adv. Mater. Res.* **2013**, *838–841*, 1685–1692. [CrossRef]
13. Li, B.; Zhang, J.; Yu, Z.; Liang, Z.; Chen, L.; Acharya, K. Climate change driven water budget dynamics of a Tibetan inland lake. *Glob. Planet. Chang.* **2017**, *150*, 70–80. [CrossRef]
14. Wu, Y.; Zheng, H.; Zhang, B.; Chen, D. Long-Term Changes of Lake Level and Water Budget in the Nam Co Lake Basin, Central Tibetan Plateau. *J. Hydrometeorol.* **2014**. [CrossRef]
15. Wang, J.; Zhu, L.; Wang, Y.; Ju, J.; Daut, G.; Li, M. Spatial variability and the controlling mechanisms of surface sediments from Nam Co, central Tibetan Plateau, China. *Sediment. Geol.* **2015**, *319*, 69–77. [CrossRef]
16. Krause, P.; Biskop, S.; Helmschrot, J.; Flügel, W.A.; Kang, S.; Gao, T. Hydrological system analysis and modelling of the Nam Co basin in Tibet. *Adv. Geosci.* **2010**, *27*, 29–36. [CrossRef]
17. Kasper, T.; Haberzettl, T.; Doberschütz, S.; Daut, G.; Wang, J.; Zhu, L.; Nowaczyk, N.; Mäusbacher, R. Indian Ocean Summer Monsoon (IOSM)-dynamics within the past 4 ka recorded in the sediments of Lake Nam Co, central Tibetan Plateau (China). *Quat. Sci. Rev.* **2012**, *39*, 73–85. [CrossRef]
18. Zhu, L.; Xie, M.; Wu, Y. Quantitative analysis of lake area variations and the influence factors from 1971 to 2004 in the Nam Co basin of the Tibetan Plateau. *Chin. Sci. Bull.* **2010**, *55*, 1294–1303. [CrossRef]
19. Tanguang, G.; Shichang, K.; Cuo, L.; Tingjun, Z.; Guoshuai, Z.; Yulan, Z.; Sillanpää, M. Simulation and analysis of glacier runoff and mass balance in the Nam Co basin, southern Tibetan Plateau. *J. Glaciol.* **2015**, *61*. [CrossRef]
20. Cheng, G.; Jin, H. Permafrost and groundwater on the Qinghai-Tibet Plateau and in northeast China. *Hydrogeol. J.* **2013**, *21*, 5–23. [CrossRef]
21. Lei, Y.; Yao, T.; Bird, B.W.; Yang, K.; Zhai, J.; Sheng, Y. Coherent lake growth on the central Tibetan Plateau since the 1970s: Characterization and attribution. *J. Hydrol.* **2013**, *483*, 61–67. [CrossRef]
22. Huang, L.; Wang, J.; Zhu, L.; Ju, J.; Daut, G. The Warming of Large Lakes on the Tibetan Plateau: Evidence From a Lake Model Simulation of Nam Co, China, during 1979–2012. *J. Geophys. Res. Atmos.* **2017**. [CrossRef]
23. Wang, X.; Zhou, A.; Sun, Z. Spatial and temporal dynamics of lakes in Nam Co Basin, 1991–2011. *J. Earth Sci.* **2016**, *27*, 130–138. [CrossRef]
24. Adnan, M.; Kang, S.; Zhang, G.; Saifullah, M.; Anjum, M.N.; Ali, A.F. Simulation and analysis of the water balance of the Nam Co Lake using SWAT model. *Water* **2019**, *11*, 1383. [CrossRef]
25. Biskop, S.; Maussion, F.; Krause, P.; Fink, M. Differences in the water-balance components of four lakes in the southern-central Tibetan Plateau. *Hydrol. Earth Syst. Sci.* **2016**, *20*, 209–225. [CrossRef]
26. Ma, N.; Szilagyi, J.; Niu, G.-Y.; Zhang, Y.; Zhang, T.; Wang, B.; Wu, Y. Evaporation variability of Nam Co Lake in the Tibetan Plateau and its role in recent rapid lake expansion. *J. Hydrol.* **2016**, *537*, 27–35. [CrossRef]
27. Du, Y.; Huang, Z.; Xie, M.; Farooq, A.; Chen, C.; Du, Y.; Huang, Z.; Xie, M.; Farooq, A.; Chen, C. Temporal Variations in the Quantity of Groundwater Flow in Nam Co Lake. *Water* **2018**, *10*, 941. [CrossRef]
28. Li, B.; Yu, Z.; Liang, Z.; Acharya, K. Hydrologic response of a high altitude glacierized basin in the central Tibetan Plateau. *Glob. Planet. Chang.* **2014**, *118*, 69–84. [CrossRef]

29. Zhang, G.; Yao, T.; Shum, C.K.; Yi, S.; Yang, K.; Xie, H.; Feng, W.; Bolch, T.; Wang, L.; Behrangi, A.; et al. Lake volume and groundwater storage variations in Tibetan Plateau's endorheic basin. *Geophys. Res. Lett.* **2017**, *44*, 5550–5560. [CrossRef]
30. Chen, J.; Chen, X.; Wang, T. Isotopes tracer research of wet sand layer water sources in Alxa Desert. *Adv. Water Sci.* **2014**, *25*, 196–206.
31. Doetsch, J.; Linde, N.; Coscia, I.; Greenhalgh, S.A.; Green, A.G. Zonation for 3D aquifer characterization based on joint inversions of multimethod crosshole geophysical data. *Geophysics* **2010**, *75*, G53–G64. [CrossRef]
32. Doro, K.O.; Leven, C.; Cirpka, O.A. Delineating subsurface heterogeneity at a loop of River Steinlach using geophysical and hydrogeological methods. *Environ. Earth Sci.* **2013**, *69*, 335–348. [CrossRef]
33. Hasan, M.; Shang, Y.; Jin, W. Delineation of weathered/fracture zones for aquifer potential using an integrated geophysical approach: A case study from South China. *J. Appl. Geophys.* **2018**, *157*, 47–60. [CrossRef]
34. Tassy, A.; Maxwell, M.; Borgomano, J.; Arfib, B.; Fournier, F.; Gilli, E.; Guglielmi, Y. Electrical resistivity tomography (ERT) of a coastal carbonate aquifer (Port-Miou, SE France). *Environ. Earth Sci.* **2014**, *71*, 601–608. [CrossRef]
35. Zaidi, F.K.; Kassem, O.M.K. Use of electrical resistivity tomography in delineating zones of groundwater potential in arid regions: A case study from Diriyah region of Saudi Arabia. *Arab. J. Geosci.* **2012**, *5*, 327–333. [CrossRef]
36. Wang, J.; Zhu, L.; Daut, G.; Ju, J.; Lin, X.; Wang, Y.; Zhen, X. Investigation of bathymetry and water quality of Lake Nam Co, the largest lake on the central Tibetan Plateau, China. *Limnology* **2009**, *10*, 149–158. [CrossRef]
37. Wang, J.; Huang, L.; Ju, J.; Daut, G.; Ma, Q.; Zhu, L.; Haberzettl, T.; Baade, J.; Mäusbacher, R.; Hamilton, A.; et al. Seasonal stratification of a deep, high-altitude, dimictic lake: Nam Co, Tibetan Plateau. *J. Hydrol.* **2020**, *584*, 124668. [CrossRef]
38. Liu, M.G. *Atlas of Physical Geography of China (Chinese Edition)*; SinoMaps Press: Beijing, China, 2010; ISBN 978-7503153716.
39. Keil, A.; Berking, J.; Mügler, I.; Schütt, B.; Schwalb, A.; Steeb, P. Hydrological and geomorphological basin and catchment characteristics of Lake Nam Co, South-Central Tibet. *Quat. Int.* **2010**, *218*, 118–130. [CrossRef]
40. Mügler, I.; Gleixner, G.; Günther, F.; Mäusbacher, R.; Daut, G.; Schütt, B.; Berking, J.; Schwalb, A.; Schwark, L.; Xu, B.; et al. A multi-proxy approach to reconstruct hydrological changes and Holocene climate development of Nam Co, Central Tibet. *J. Paleolimnol.* **2010**, *43*, 625–648. [CrossRef]
41. Wang, J.; Zhu, L.; Wang, Y.; Ju, J.; Xie, M.; Daut, G. Comparisons between the chemical compositions of lake water, inflowing river water, and lake sediment in Nam Co, central Tibetan Plateau, China and their controlling mechanisms. *J. Great Lakes Res.* **2010**, *36*, 587–595. [CrossRef]
42. Kapp, J.L.D.A.; Harrison, T.M.; Kapp, P.; Grove, M.; Lovera, O.M.; Lin, D. Nyainqentanglha Shan: A window into the tectonic, thermal, and geochemical evolution of the Lhasa block, southern Tibet. *J. Geophys. Res. Solid Earth* **2005**, *110*, 1–23. [CrossRef]
43. Schütt, B.; Berking, J.; Frechen, M.; Yi, C. Late Pleistocene Lake Level Fluctuations of the Nam Co, Tibetan Plateau, China. *Z. Geomorphol. Suppl. Issues* **2008**, *52*, 57–75. [CrossRef]
44. Wang, L.; Yi, C.; Xu, X.; Schütt, B.; Liu, K.; Zhou, L. Soil Properties in Two Soil Profiles from Terraces of the Nam Co Lake in Tibet, China. *J. Mt. Sci.* **2009**. [CrossRef]
45. Development Research Center of China, G.S. (National G.A. Geological and mineral resources map Nam Co). Available online: http://www.ngac.org.cn/ (accessed on 17 August 2019).
46. Jarvis, A.; Reuter, H.I.; Nelson, A.; Guevara, E. Hole-filled SRTM seamless SRTM data Version 4, International Centre for Tropical Agriculture (CIAT). Available online: http://srtm.csi.cgiar.org (accessed on 29 July 2019).
47. Cuo, L.; Zhang, Y.; Gao, Y.; Hao, Z.; Cairang, L. The impacts of climate change and land cover/use transition on the hydrology in the upper Yellow River Basin, China. *J. Hydrol.* **2013**, *502*, 37–52. [CrossRef]
48. Vukovic, M.; Soro, A. *Determination of Hydraulic Conductivity of Porous Media from Grain-Size Composition*; Water Resources Publications: Littleton, CO, USA, 1992.
49. Barr, D.W. Coefficient of Permeablity Determined By Measurable Parameters. *Ground Water* **2001**, *39*, 356–361. [CrossRef]
50. Coldewey, W.G.; Göbel, P. Güttler Untersuchungen zur Bestimmung der Gebirgsdurchlässigkeit im Rahmen der Planung und Beurteilung von Deponiestandorten in festen und wechselfesten Gesteinen. *Dmt Ber. Aus Forsch. Und Entwickl.* **2004**, *154*, 98.
51. Hvorslev, M.J. Time lag and soil permeability in ground water observations. *U.S. Army Corps Eng. Waterw. Exp. Stn. Bull.* **1951**, *36*, 1–50.
52. Schlichting, E.; Blume, H.-P.; Stahr, K. *Bodenkundliches Praktikum*, 2nd ed.; Blackwell Wissenschafts-Verlag: Berlin, Germany, 1995.
53. Jahn, R.; Blume, H.P.; Asio, V.B.; Spaargaren, O.; Schad, P. *FAO Guidelines for Soil Description*; FAO: Rome, Italy, 2006; ISBN 9251055211.
54. Devlin, J.F. HydrogeoSieveXL: An Excel-based tool to estimate hydraulic conductivity from grain size analysis. *Hydrogeol. J.* **2015**. [CrossRef]
55. Reynolds, M.J. *An Introduction to Applied and Environmental Geophysics*, 2nd ed.; Wiley: Hoboken, NJ, USA; Oxford, UK; Chichester, UK, 2011; ISBN 9780471485353.
56. Hördt, A.; Schrott, L.; Hoffmann, T.; Berthling, I.; Melvold, K.; Delaloye, R.; Lambiel, C.; Ishikawa, M.; Harada, K.; Dobin-ski, W. *Applied Geophysics in Periglacial environments*; Hauck, C., Kneisel, C., Eds.; Cambridge University Press: New York, NY, USA, 2008; ISBN 9780511535628. [CrossRef]
57. Loke, M.H.; Barker, R.D. Rapid least-squares inversion of apparent resistivity pseudosections by a quasi-Newton method1. *Geophys. Prospect.* **1996**, *44*, 131–152. [CrossRef]

58. Archie, G. The Electrical Resistivity Log as an Aid in Determining Some Reservoir Characteristics. *Pet. Trans. Aime* **1942**, *146*, 54–62. [CrossRef]
59. Kovalevsky, V.S.; Kruseman, G.P.; Rushton, K.R. *Groundwater Studies: An International Guide for Hydrogeological Investigations*; Unesco: Paris, France, 2004; ISBN 9292200054.
60. Oyeyemi, K.D.; Aizebeokhai, A.P.; Ndambuki, J.M.; Sanuade, O.A.; Olofinnade, O.M.; Adagunodo, T.A.; Olaojo, A.A.; Adeyemi, G.A. Estimation of aquifer hydraulic parameters from surficial geophysical methods: A case study of Ota, Southwestern Nigeria. *Iop Conf. Ser. Earth Environ. Sci.* **2018**, 173. [CrossRef]
61. Lehmkuhl, F.; Klinge, M.; Lang, A. Late Quaternary glacier advances, lake level fluctuations and aeolian sedimentation in Southern Tibet. *Z. Geomorphol. N.F. Suppl.* **2002**, *126*, 183–218.
62. Vessia, G.; Di Curzio, D. *Lacustrine Deposits—Encyclopedia of Engineering Geology*; Bobrowsky, P., Marker, B., Eds.; Springer International Publishing: Cham, Switzerland, 2018; pp. 1–6. ISBN 978-3-319-12127-7. [CrossRef]
63. Appel, D.; Habler, W. *Quantifizierung der Wasserdurchlässigkeit von Gesteinen als Voraussetzung für die Entwicklung von Kriterien zur Grundwasserbewegung Phase 2: Auswertung der Datensätze für die Kriterienentwicklung Anhang und Datenbank "Gebirgsdurchlässigkeit" (auf CD-ROM)*. Available online: https://docplayer.org/15628493-Datenbank-gebirgsdurchlaessigkeit-auf-cd-rom.html (accessed on 3 August 2020).
64. Palacky, G. Resistivity Characteristics of Geological Targets. In *Electromagnetic Methods in Applied Geophysics-Theory*; Nabighian, M., Ed.; Society of Exploration Geophysicists Tulsa: Tulsa, OK, USA, 1987; pp. 53–129.
65. Wilhelm, S.; Mountains, B.F. Application of Electrical Resistivity Tomography (ERT) Together with Tracer Data to Identify Hydrological Process Areas at a Surface Water/Groundwater Test Site. Ph.D. Thesis, Institut für Hydrologie, Albert-Ludwigs Universität Freiburg, Freiburg, Germany, 2004.
66. Domenico, P.A.; Schwartz, F.W. *Physical and Chemical Hydrogeology*; Wiley: Hoboken, NJ, USA, 1998; ISBN 0471597627.
67. Tian, K.; Liu, J.; Kang, S.; Campbell, I.B.; Zhang, F.; Zhang, Q.; Lu, W. Hydrothermal pattern of frozen soil in Nam Co lake basin, the Tibetan Plateau. *Environ. Geol.* **2009**, *57*, 1775–1784. [CrossRef]
68. Bian, C.Y.; Zuo, Z.K.; Qiao, W.G.; Fan, X.D.; Wang, Z.L.; Dai, S.W.; Meng, Y.M.; Wu, W.X.; Wang, Q.H. Chinese regional hydrogeology survey report—Anduo Quad (in Chinese). *Geol. Min. Bur. Xining China* **1990**, 138.
69. Shang, J.Y.; Sun, C.Y.; He, M.Y.; Yan, S.B. Qinghai-Tibet (Golmud-Anduo) hydrogeology (in Chinese). *Qinghai Prov. Geol. Bur. Xining China* **1977**, 120.